nanomaterials

MDPI

Article

Study on the Effects of a π Electron Conjugated Structure in Binuclear Metallophthalocyanines Graphene-Based Oxygen Reduction Reaction Catalysts

Gai Zhang [1,*], Bulei Liu [1], Yufan Zhang [1], Tiantian Li [2], Weixing Chen [1] and Weifeng Zhao [1,*]

[1] School of Materials Science and Chemical Engineering, Xi'an Technological University, Xi'an 710021, China; gaomin@st.xatu.edu.cn (B.L.); zhangyufan@st.xatu.edu.cn (Y.Z.); chenwx@xatu.edu.cn (W.C.)

[2] Key Laboratory of Synthetic and Natural Functional Molecule Chemistry of Ministry of Education, College of Chemistry & Material Chemistry, Northwest University, Xi'an 710069, China; 2015116027@stumail.nwu.edu.cn

* Correspondence: zhanggai@xatu.edu.cn (G.Z.); zhaoweifeng@xatu.edu.cn (W.Z.); Tel./Fax: +86-029-86173324 (G.Z. & W.Z.)

Received: 3 April 2020; Accepted: 9 May 2020; Published: 15 May 2020

Abstract: The high overpotentials for oxygen reduction reaction (ORR) create an extremely negative impact on the energy efficiency of the air-based battery systems. To overcome this problem, binuclear ball-type metallophthalocyanines containing methoxy substituents ($M_2Pc_2(EP)_4$, M = Fe(II), Co(II) and Zn(II)) were wrapped with polystyrene sodium sulfonate (PSS) modified graphene oxide (GO), using a facilely "solvothermal π-π assembly" method to prepare $M_2Pc_2(EP)_4$/PSS-Gr composites. Compared with the commercial Pt/C catalysts, the $M_2Pc_2(EP)_4$/PSS-Gr composites enhanced the catalytic activity of oxygen reduction reaction. The π electron conjugated structure of the MN_4-type phthalocyanine macrocyclic system strongly influenced the one-step four-electron electrocatalytic process of the $M_2Pc_2(EP)_4$/PSS-Gr composites. Moreover, the π-π interactions between the $M_2Pc_2(EP)_4$ and PSS-Gr dramatically enhanced the π electron density in the conjugated structure and oxygen could be reduced more easily. The electrocatalytic activity test was displayed in the order of $Fe_2Pc_2(FP)_4$/PSS-Gr > $Co_2Pc_2(EP)_4$/PSS-Gr > $Zn_2Pc_2(EP)_4$/PSS-Gr. The results indicated that the catalytic performance of $M_2Pc_2R_n$ could be enhanced by the modification of π electron conjugated structure of $M_2Pc_2(EP)_4$ and carbon materials.

Keywords: metallophthalocyanines; PSS-Graphene; π-π interactions; ORR

1. Introduction

With the exhausting of traditional energy sources and increasing concerns of environmental pollution, it is urgent to explore and utilize clean energy. Fuel cells have become the research hotspots for new energy development because of their low cost, simple structure, special energy density and other merits [1–3]. Nevertheless, the high overpotentials for the oxygen reduction reactions create an extremely negative impact on the energy efficiency of air-based battery systems [4]. Although Pt and its alloys contribute significantly in decreasing the overpotential of oxygen reduction reaction (ORR) because of their high catalytic activity, they are limited in the scarcity of reserves, high price and lack of excellent methanol resistance [5]. To overcome this problem, extensive efforts have been implemented to study low-cost, non-precious metal substitute catalysts for Pt/C catalysts [6,7]. Specially, many reports have pointed out that the ability to carry oxygen molecules plays a key role in the ORR process [8,9]. Among the large variety of metal macrocycles, metal-N_4-chelates, like metalloporphyrin

(MPs) and metallophthalocyanine (MPcs), which have an 18 π electrons conjugated structure, have the biomimetic oxygen carrier functions similar to the naturally occurring hemeproteins [10]. Due to the delocalization effect and weakly bonding character of π electron clouds in a conjugated structure, the metal-N_4-chelates with π electron conjugated structure could be oxidized and reduced much more easily, establishing them as a promising precursor for preparing ORR catalysts [11–13]. Compared with MPs, the periphery of the benzene ring of phthalocyanines can be modified with a variety of substituents, giving MPcs a variety of chemical structures and properties [14–16]. The chemical natures of the ligand and the central ion strongly influence the catalytic properties of the metal-N_4-chelates macrocycles. In the ORR process, O_2 is coordinated to the M of MPcs and the electrons then migrate from the MPcs to O_2 to form adduct MPc-O_2^- [17,18]. Considering a high π electron density of the conjugated structure, metallophthalocyanines have an excellent catalytic activity for oxygen reduction reaction [19–21].

In recent years, a new class of ball-type M_2Pc_2 compounds containing two metal centrals has drawn much attention because of its attractive structure [22,23]. Both the face-to-face monomer distance and the d filling of the metal central ions can significantly affect the ball-type Pcs' physical and chemical behavior [24,25]. For the M_2Pc_2 with a strong ligand-field effects of MN_4-chelates, the catalytic activity is mainly affected by the chemical structure of the phthalocyanines, the radius and the d-filling of the metal central ions [26]. In addition, the presence of bridging units including electronegative groups highly enhanced catalytic activity of the phthalocyanines. The multiple electron-withdrawing substituents on the periphery of metal Pcs increased their catalytic activity [25]. The results pointed out that the possibility of the increase of the catalytic performance by the modification of the main M_2Pc_2 skeleton, and encouraged us to design phthalocyanine compound containing methoxy substituents. Furthermore, reports have also pointed out that MPc loaded on carbon materials is conducive to enhance the catalytic activity for the oxygen reduction reaction [27,28]. Graphene oxide has a high conductivity, excellent electron mobility and relatively high theoretical specific surface areas, establishing itself as a good candidate to provide a pathway for fast electron transferring and to prevent the aggregation of MPcs nanoparticles [29,30]. It has demonstrated that the catalytic activity of the π electron conjugated structure towards oxygen reduction reaction are related to the strong π-π supramolecular interaction between MPc compounds and graphene, which promote electron transfer between them leading to an apparent improvement for the oxidative reactions [31–34]. However, pristine GO possesses few proton-conducting groups, which negatively enhances the conductivity of GO. Therefore, grafting GO with a sulfonated group (-SO_3H; PSS-Gr) using various methods has been studied, as this strategy not only improved the conductivity of the GO, but also enabled the better dispersibility of GO [35].

Some studies have provided valuable mechanistic insights for the formation of M_2PcR_n-O_2 intermediates. However, the study on the effects of the π electron conjugated structure and the π-π interactions between the $M_2Pc_2(EP)_4$ and PSS-Gr generally restrict the design of the $M_2Pc_2R_n$-based catalysts. In this work, composites of binuclear ball-type metallophthalocyanines with methoxy substituents ($M_2Pc_2(EP)_4$, M = Fe(II), Co(II) and Zn(II)) were loaded on the surface of PSS-Graphene (PSS-Gr), to enhance the catalytic activity and stability for ORR based on the π electron conjugated structure of the MN_4-type phthalocyanine macrocyclic system, and the π-π supramolecular interaction between MPc nanoparticles and graphene.

2. Experimental

2.1. Materials

4, 4-bis (4-hydroxyphenyl) pentanoic acid (98%) and 4-nitrophthalonitrile (99%) were purchased from Aladdin (Shanghai, China). The other chemicals were of analytical grade and were used without further purification. The target $M_2Pc_2(EP)_4$ compounds were prepared by taking bisphthalonitrile and the corresponding metal salts (M = Fe(II), Co(II), and Zn(II)) as the raw materials in the dimethylaminoethanol (DMAE). This was done according to the literature [25].

Preperation of $M_2(II)Pc_2(EP)_4$: Bisphthalonitrile (0.56 g, 1.02 mmol), $Zn(OAc)_2$ $2H_2O$ (0.112 g, 0.52 mmol) and 4 mL DMAE were poured into a Teflon-lined autoclave at 220 °C for 4 h (Figure 1). The reaction mixture was then poured into methanol to produce a precipitate, and the precipitate was washed sequentially with acetic acid, water and methanol. The crude product was then dissolved in DMF and reprecipitated by gradually adding methanol to the solution. The precipitate was washed again as in the previous method followed by centrifugation and dried at 100 °C in an oven.

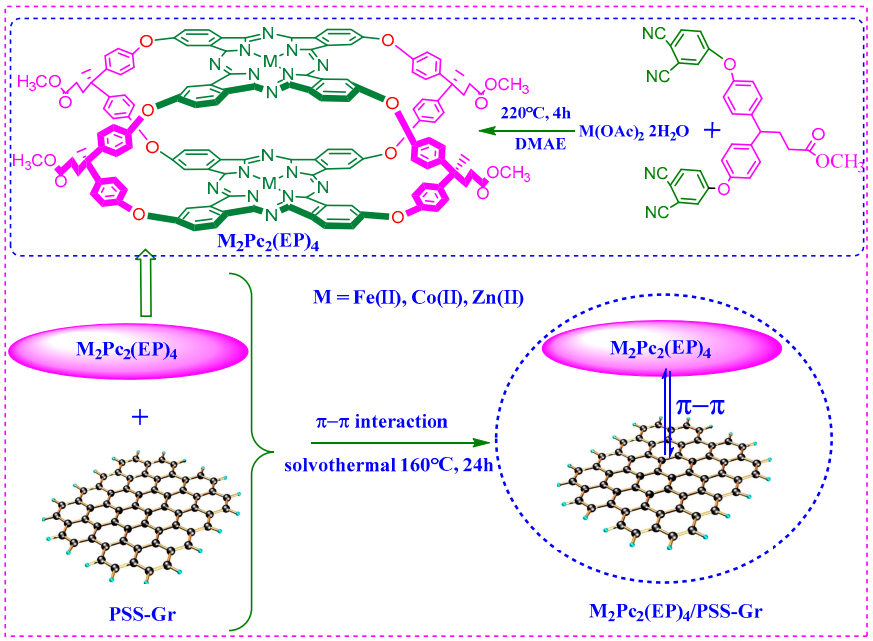

Figure 1. Schematic illustration of the preparation process for the $M_2Pc_2(EP)_4$/polystyrene sodium sulfonate modified graphene (PSS-Gr) composites.

[2′,10′,16′,24′-{Tetrakis-4,4′-bis (4- (3-cyano-4-isocyanophenoxy) phenyl) pentanoate diphthalocyaninato) dizinc (II)]: $Zn_2(II)Pc_2(EP)_4$ (0.3815 g, yield 64.21%), green solid, m.p. > 300 °C. IR (KBr) ν_{max}/cm^{-1}: 1715 ($\nu_{C=O}$); 1381 ($\nu_{C=C}$); 892 (ν_{M-N}); 2972, 1009 ($\nu_{C-H(Pc)}$), 1229 ($\nu_{Ar-O-Ar}$), 740 (ν_{Pc}). UV-Vis (DMF) λ_{max}/nm: B band: 267, 354; Q band: 612, 677. Anal. Cald. for $C_{32}H_{16}N_8Zn$: C, 69.78; H, 4.10; N, 9.58; Found: C, 69.21; H, 4.54; N, 9.29.

[2′,10′,16′,24′-{Tetrakis-4, 4′-bis (4- (3-cyano-4-isocyanophenoxy) phenyl) pentanoate diphthalocyaninato) diiron (II)]: $Fe_2(II)Pc_2(EP)_4$ (0.2120 g, yield 36.64%), olive green solid, m.p. > 300 °C. IR (KBr) ν_{max}/cm^{-1}: 1713 ($\nu_{C=O}$); 1401 ($\nu_{C=C}$); 874 (ν_{M-N}); 2970, 1011 ($\nu_{C-H(Pc)}$), 1234 ($\nu_{Ar-O-Ar}$), 752 (ν_{Pc}). UV-Vis (DMF) λ_{max}/nm: B band: 267, 323; Q band: 621, 668. Anal. Cald. for $C_{32}H_{16}N_8Fe$: C, 70.07; H, 4.12; N, 9.62; Found: C, 69.68; H, 3.63; N, 9.27.

[2′,10′,16′,24′-{Tetrakis-4, 4′-bis (4- (3-cyano-4-isocyanophenoxy) phenyl) pentanoate diphthalocyaninato) dicobalt (II): $Co_2(II)Pc_2(EP)_4$(0.3021 g, yield 51.52%), dark blue solid, m.p. > 300 °C. IR (KBr) ν_{max}/cm^{-1}: 1707 ($\nu_{C=O}$); 1387 ($\nu_{C=C}$); 891 (ν_{M-N}); 2970, 1011 ($\nu_{C-H(Pc)}$), 1231 ($\nu_{Ar-O-Ar}$), 745 (ν_{Pc}). UV-Vis (DMF) λ_{max}/nm: B band: 268, 362; Q band: 668. Anal. Cald. for $C_{32}H_{16}N_8Co$: C, 69.97; H, 4.11; N, 9.61; Found: C, 69.55; H, 4.56; N, 9.19.

2.2. Characterization

Transmission electron microscopy (TEM) analysis was performed on a JEOL JEM-2010 electron microscope at 200 kV. The system consists of a vertical SEM column that was situated at 36° relative to the FIB column, operating at 3 kV to optimize surface sensitivity. The IR spectra were recorded on a Germany Bruker Vertex70 spectrometer (Bruker, Karlsruhe, Germany). The UV-vis absorbance was

recorded on a UV/visible spectrophotometer (UV-1600, Shanghai, China) using a quartz cell with a path length of 10 mm at room temperature. X-ray photoelectron spectroscopy (XPS) was measured using an Axis Ultra spectrometer with an Al (Mono) Kα X-ray source (1486.6 eV). The binding energies (BE) were normalized to the signal for adventitious carbon at 284.8 eV. The electrocatalytic performance was evaluated by an electrochemical workstation CHI 660E (Shanghai CHENHUA Company, Shanghai, China) and a Pine Instrument Company AF-MSRCE modulator rate rotator (Grove, PA, USA) in a 0.1 M KOH solution, separately.

2.3. Synthesis

2.3.1. Polystyrene Sodium Sulfonate Modified Graphene (PSS-Gr) Preparation

Graphene oxide (GO), obtained from Aladain Co. Ltd. (Shanghai, China) was dispersed in 100 mL distilled water with an ultrasonic technique, followed by the addition of 1 g of sodium polystyrene sulfonate at room temperature, and stirred for 12 h. Then, 2 mL of hydrazine hydrate was then added. The crude products were washed with deionized water, ethanol and n-pentanol, followed by centrifugation and then drying at 100 °C.

2.3.2. Preparation of $Fe_2Pc_2(EP)_4$/PSS-Gr

The $Fe_2Pc_2(EP)_4$/PSS-Gr composites were synthesized by a facile "solvothermal π-π assembly" method, using PSS-Gr and $Fe_2Pc_2(EP)_4$ as the precursors (Figure 1). In brief, 0.1503 g of PSS-Gr powder was dispersed in 10 mL of DMF solution with an ultrasonic technique for 10 min, followed by the addition of 0.1100 g metallophthalocyanine $Fe_2Pc_2(EP)_4$. The resulting solution was ultrasonically dispersed for 2 h. Nitrogen gas was then bubbled into the mixture to remove oxygen and was then poured into a Teflon-lined autoclave at 160 °C for 24 h. All of the crude products were washed with DMF, deionized water, ethanol and n-pentanol, followed by centrifugation and drying at 100 °C in an oven.

The $Co_2Pc_2(EP)_4$/PSS-Gr and $Zn_2Pc_2(EP)_4$/PSS-Gr composites were prepared under the same conditions.

2.4. Evaluation of the Electrocatalytic Activity

The electrocatalytic performance of $M_2Pc_2(EP)_4$/PSS-Gr composites for the oxygen reduction reaction was measured by cyclic voltammetry (CV) and rotating disk electrode (RDE) techniques in a 0.1 M NaOH solution at room temperature. Specifically, the modified glassy carbon electrode is used as a working electrode. The reference electrode is saturated calomel electrode (SCE) and the platinum (Pt) wire electrode is used as counter electrode, respectively. The cyclic voltammetry tests were investigated in an O_2-saturated 0.1 M NaOH solution with the scan rate of 100mV s^{-1}. The rotating disk electrode (RDE) test was measured with a glassy carbon electrode (5 mm diameter) in O_2-saturated 0.1 M NaOH solution under quasistationary conditions (5 mV·s^{-1} sweep rate) at 25 °C. The rotating disk electrode (RDE) was performed on a CHI 660E electrochemical workstation with an AF-MSRCE modulator rate rotator (Pine Instrument Company) using a standard three-electrode system. A platinum ring electrode and glassy carbon disk (5.61 mm diameter) was selected as the working electrode. The collection efficiency of the platinum ring was 37%.

3. Results and Discussion

3.1. Morphology and Structure of $M_2Pc_2(EP)_4$/PSS-Gr Composites

The surface morphology of the $M_2Pc_2(EP)_4$/PSS-Gr composites was studied by SEM and TEM images. As illustrated in Figure 2, a wrinkled paper-like feature was observed for the PSS-Gr, indicating a typical feature of the graphene sheet. In contrast to the TEM micrograph of PSS-Gr that appears transparent (Figure 2b), numerous dark particles of $M_2Pc_2(EP)_4$, as indicated by the white arrow, were

observed on the PSS-Gr layer from the TEM image of the $M_2Pc_2(EP)_4$/PSS-Gr composites. It can be seen that $M_2Pc_2(EP)_4$ nanoparticles were dispersed uniformly on the PSS-Gr surface.

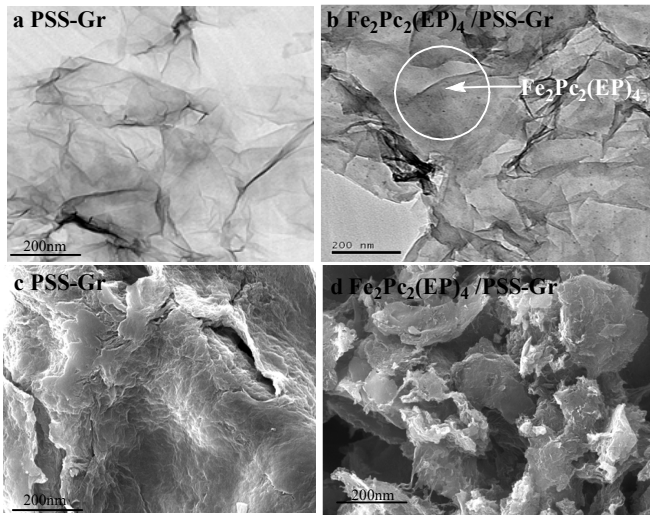

Figure 2. TEM and SEM images of PSS-Gr and $Fe_2Pc_2(EP)_4$/PSS-Gr; (**a**), (**c**) TEM and SEM images of PSS-Gr; (**b**), (**d**) TEM and SEM images of $Fe_2Pc_2(EP)_4$/PSS-Gr.

The UV-Vis spectra of the $Fe_2Pc_2(EP)_4$/PSS-Gr composites is shown in Figure 3. The "Q-band" of $Fe_2Pc_2(EP)_4$ appeared at around 668 nm, because of the π-π originating from the HOMO (a_{1u} and a_{2u}) to the LUMO orbitals (e_g) [25]. The absorption at 621 nm is attributed to the dimmers of $Fe_2Pc_2(EP)_4$. The spectrum of the PSS-Gr did not exhibit any obvious absorption peaks from 300 to 900 nm, while that of the $Fe_2Pc_2(EP)_4$/PSS-Gr composites in DMF showed an absorption peak at 741 nm. Compared with the $Fe_2Pc_2(EP)_4$, the absorption of the $Fe_2Pc_2(EP)_4$/PSS-Gr samples are red shifted from 668 nm to 741 nm, and the absorption of $Fe_2Pc_2(EP)_4$ dimmers at 621 nm disappeared. This suggests a strong π-π supramolecular interaction between the $Fe_2Pc_2(EP)_4$ and PSS-GR [36–38], which will prevent the aggregation of $Fe_2Pc_2(EP)_4$ compounds and enhance the π electron density in conjugated structure. Moreover, the strong π-π supramolecular interaction facilitates electron transfer between them, leading to the observed improvement for the oxygen reduction reaction.

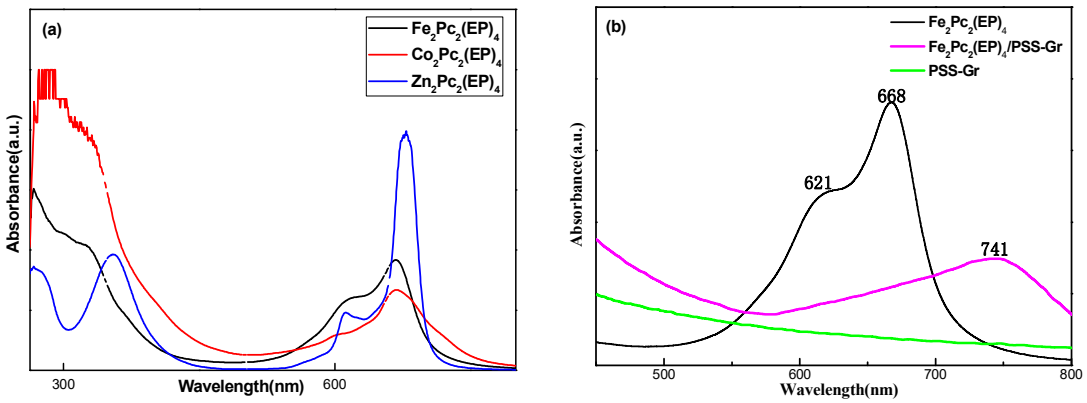

Figure 3. (**a**) UV-Vis spectra of $Fe_2Pc_2(EP)_4$, $Co_2Pc_2(EP)_4$, and $Zn_2Pc_2(EP)_4$, and (**b**) UV-vis spectra of $Fe_2Pc_2(EP)_4$/PSS-Gr, $Fe_2Pc_2(EP)_4$ and PSS-Gr.

To further illustrate the composition and chemical status of the as-prepared catalysts, the $Fe_2Pc_2(EP)_4$/PSS-Gr were also analyzed by XPS. Figure 4a displays the XPS survey spectra of GO, PSS-Gr, $Fe_2Pc_2(EP)_4$, and $Fe_2Pc_2(EP)_4$/PSS-Gr composites. The results showed that the $Fe_2Pc_2(EP)_4$/PSS-Gr catalysts are composed of O, C, N and Fe elements, which further confirms the existence of $Fe_2Pc_2(EP)_4$

in the as-prepared samples. Compared with GO, the obviously decreasing O content for PSS-Gr indicates that a relatively high degree of reduction had been achieved during the hydrothermal process. The high-resolution N1s spectrum of the composite $Fe_2Pc_2(EP)_4$ and $Fe_2Pc_2(EP)_4$/PSS-Gr are shown in Figure 4c,d. The two asymmetric broad peaks of N1s for $Fe_2Pc_2(EP)_4$ are located at 398.1 eV and 399.4 eV, which correspond to the signals of C-N and C = N of pyrrolic ring in the phthalocyanine macrocycle, respectively [39,40]. What is more interesting is that the binding energy values of N1s in the $Fe_2Pc_2(EP)_4$/PSS-Gr composites are obviously higher than those of pure $Fe_2Pc_2(EP)_4$, which confirms a strong interaction between $Fe_2Pc_2(EP)_4$ and PSS-Gr.

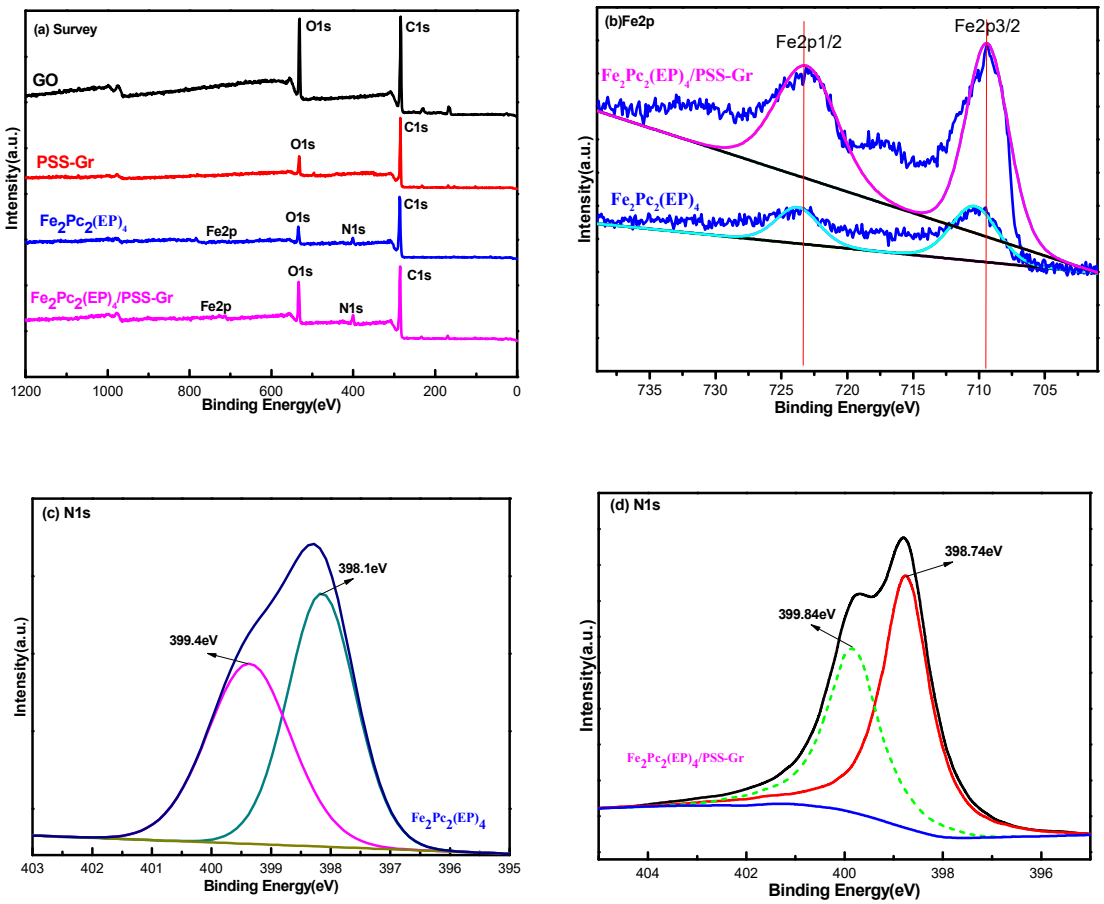

Figure 4. X-ray photoelectron spectroscopy (XPS) spectra of $Fe_2Pc_2(EP)_4$/PSS-Gr; (**a**) XPS survey spectra of GO, PSS-Gr, $Fe_2Pc_2(EP)_4$ and $Fe_2Pc_2(EP)_4$/PSS-GR; (**b**), (**c**), (**d**) High resolution of Fe2p, N1s XPS spectra of $Fe_2Pc_2(EP)_4$ and $Fe_2Pc_2(EP)_4$/PSS-Gr.

The high-resolution Fe2p spectrum of the catalysts is shown in Figure 4b. The peaks of Fe2p for $Fe_2Pc_2(EP)_4$ are located at 723.9 eV and 710.6 eV, which correspond to the signals of $Fe2p_{1/2}$ and $Fe2p_{3/2}$ in the bivalent oxidation state, respectively. However, the binding energy values of Fe2p in the composites of $Fe_2Pc_2(EP)_4$/PSS-Gr are obviously lower than those of pure $Fe_2Pc_2(EP)_4$ [19]. The shift again confirms a π-π supramolecular interaction between $Fe_2Pc_2(EP)_4$ and PSS-Gr, indicating the as-prepared composites of $Fe_2Pc_{2(}EP)_4$ and PSS-Gr tend to form a hetero structure, rather than a physical mixture.

3.2. Effects of π Electron Conjugated Structure for ORR

The electrocatalytic activity of the $M_2Pc_2(EP)_4$/PSS-Gr composites for ORR were first tested by the technique of CV. As shown in Figure 5, the ORR peak currents in the voltammograms showed that $M_2Pc_2(EP)_4$/PSS-Gr composites interact well with O_2 through the redox-active character of the

M^{2+} cores. The π electron conjugated structure of the MN_4-type phthalocyanine macrocyclic system strongly influences the redox-active character of the M^{2+} cores. Therefore, because of the d filling t_{2g}^6 e_g^0 of Fe(II) with a fully filled t_{2g} and unoccupied e_g orbitals, the central metal Fe(II) was favored to coordinate with dioxygen, and was oxidized to Fe(III) much more easily in the redox process [17]. The results showed that the Fe(II)/Fe(III) reduction peak current of O_2 commenced at lower positive potentials (−0.15 V vs. SCE) than that of the Pt/C (−0.17 V vs. SCE). When the Fe(II)/Fe(III) redox transition occurs at low positive potentials, highly acidic Fe(III) species well interact well with dioxygen and provide a relatively low overpotential for ORR. Moreover, the reduction potential of Fe(III)/Fe(II) (−0.15 V vs. SCE) is more positive than that of Co(III)/Co(II) (−0.21 V vs. SCE) and Zn(III)/Zn(II)(−0.59V vs. SCE). The results indicated that the electrocatalytic activity is closely related to their radius and d filling of the active center ions. $Zn_2Pc_2(EP)_4$/PSS-Gr shows a relatively low catalytic activity for ORR because of the fully filled t_{2g}^6 and e_g^4 orbitals, which make Zn(II) difficult to be oxidized to Zn(III) by the O_2 in the vertical direction of the conjugate plane in a strong ligand-field. Whereas the ORR process occurs only on the phthalocyanine ring, and is independent of the central metal Zn(II).

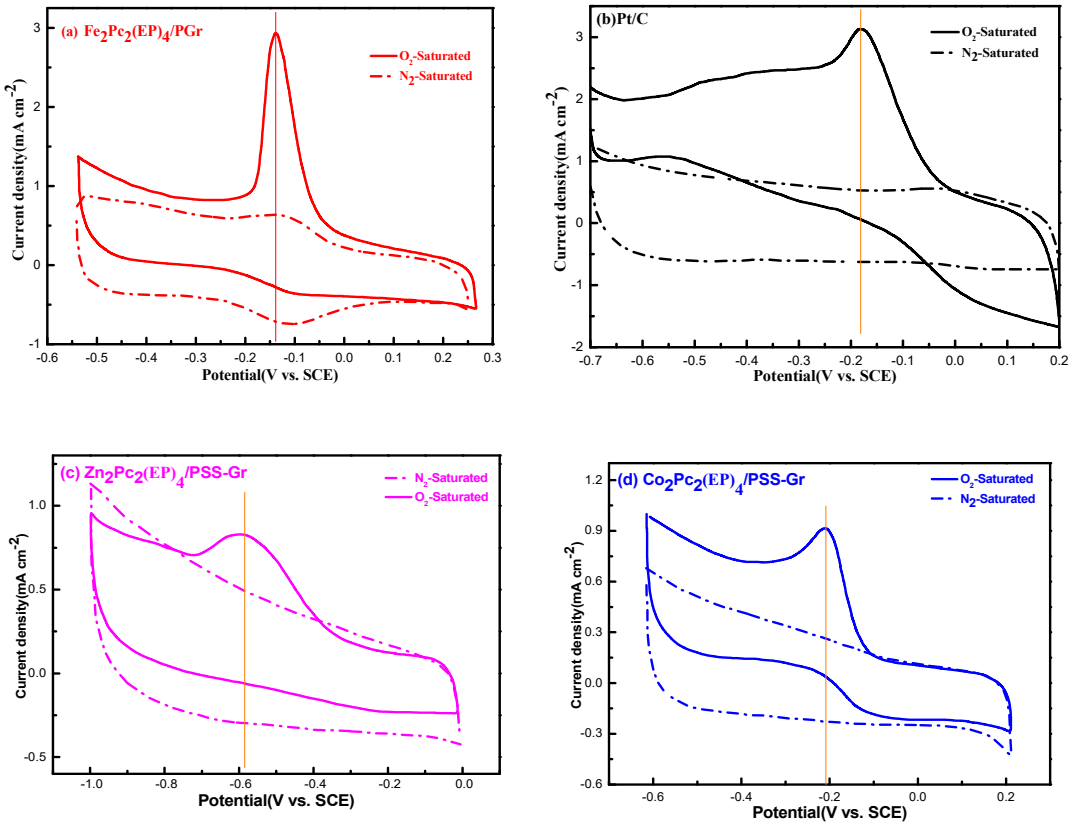

Figure 5. Cyclic Voltammograms curve of $M_2Pc_2(EP)_4$/PSS-Gr and Pt/C catalysts on glassy carbon electrodes; (**a**), (**b**), (**c**), (**d**) CV curve of $Fe_2Pc_2(EP)_4$/PSS-Gr, Pt/C, $Zn_2Pc_2(EP)_4$/PSS-Gr, and $Fe_2Pc_2(EP)_4$/PSS-Gr;

In order to further investigate the influence of the catalysts structures for ORR, the linear sweep voltammetry (LSV) measurement was performed on a rotating disk electrode (RDE) at a scanning rate of 5 mV^{-1} in O_2-saturated 0.1 M KOH solution with the rotational speed from 400 rpm to 2500 rpm. A comparison of the LSV results was recorded at 1600 rpm rotational speed using Pt/C, PSS-Gr, $Fe_2Pc_2(EP)_4$ and $Fe_2Pc_2(EP)_4$/PSS-Gr modified electrodes individually. The onset potential (E_0) and the limiting diffusion current density (J_l) were taken as measures of the catalytic activity. Compared with the ORR potentials of PSS-Gr (−0.17 V vs. SCE) and $Fe_2Pc_2(EP)_4$ (−0.27 V vs. SCE), the onset potential of $Fe_2Pc_2(EP)_4$/Gr was positively shifted to −0.09 V, which is close to the onset potential of Pt/C (−0.07

V). The results indicated that the electrocatalytic activity of $Fe_2Pc_2(EP)_4$/PSS-Gr was enhanced by the π-π supramolecular interaction between $Fe_2Pc_2(EP)_4$ compounds and PSS-Gr, which enhance the π electron density in $Pc_2(EP)_4$ conjugated structure, leading to an observed improvement for the oxygen reduction reaction [41,42].

Furthermore, it is well known that a one-step four-electron process has more excellent electrocatalytic performances than the two-electron process for an oxygen reduction reaction [43–45]. The total electron transfer number (n) in the ORR reaction is calculated by the Koutecky-Levich (K-L) equation given below (1) and (2):

$$\frac{1}{J} = \frac{1}{JK} + \frac{1}{JL} = \frac{1}{nFKC_o} + \frac{1}{B\omega^{1/2}}, \quad (1)$$

$$B = 0.62nFC_o(D_0)^{2/3}\nu^{-1/6}, \quad (2)$$

where J (mA/cm^2) is the measured current density; J_K and J_L (mA/cm^2) are the kinetic and diffusion-controlled current density, respectively; ω is the angular velocity of the rotating disk (ω = 2πN, N is the linear rotation speed in rpm); n is the total number of electron transferred per oxygen molecule in the ORR reaction; F is the Faraday constant; C_0 is the bulk oxygen concentration; D_0 is the diffusion coefficient of oxygen; and ν is the kinematic viscosity of the electrolyte.

The K-L points (J^{-1} vs. $\omega^{-1/2}$) of $M_2Pc_2(EP)_4$/PSS-Gr at different voltages an exhibited excellent linearity and the slope is consistent (Figure 6). The linearity of the K-L plots and the near parallelism of the fitting lines suggested first-order reaction kinetics for ORR. The electron transfer number n is further calculated by the Koutecky-Levich (K-L) equation. The n for $Fe_2Pc_2(EP)_4$/PSS-Gr was 3.89 at the voltage range from −0.4 V to −0.7 V, and was similar in the redox process at different potentials. The results indicated that the ORR mainly proceeded a one-step four electron process for $Fe_2Pc_2(EP)_4$/PSS-Gr which is similar to the Pt/C catalysts.

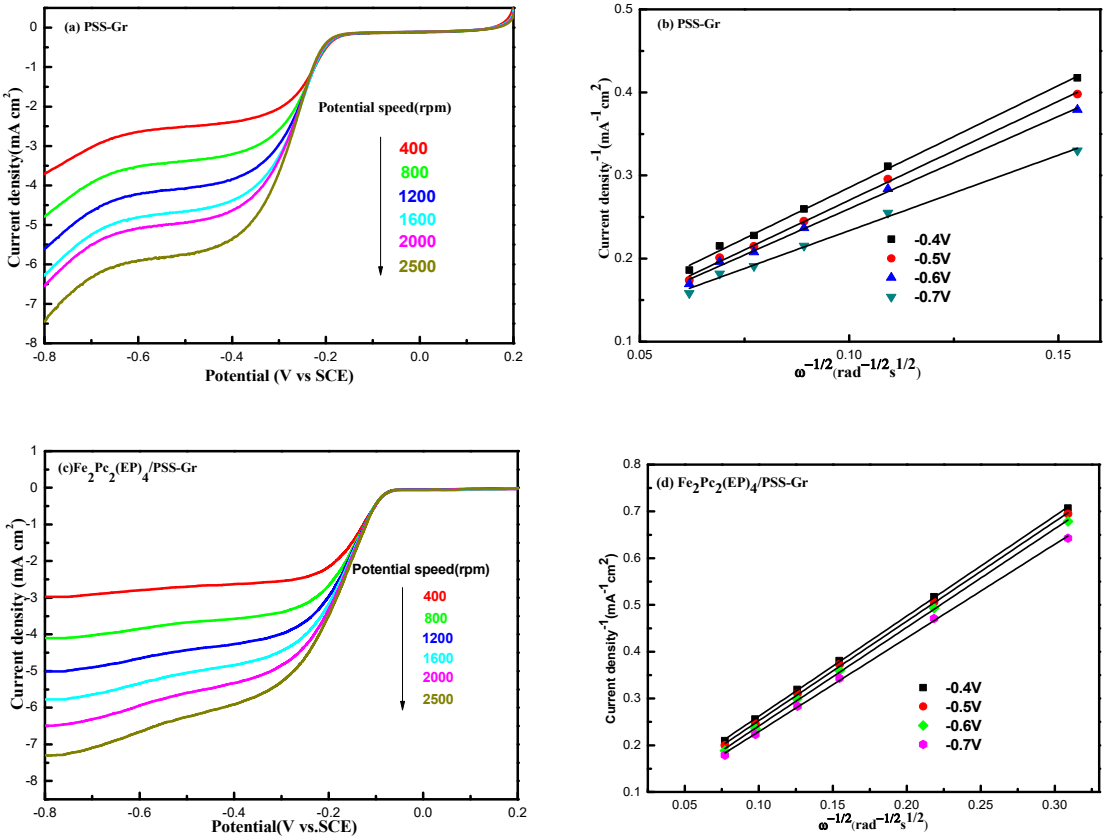

Figure 6. *Cont.*

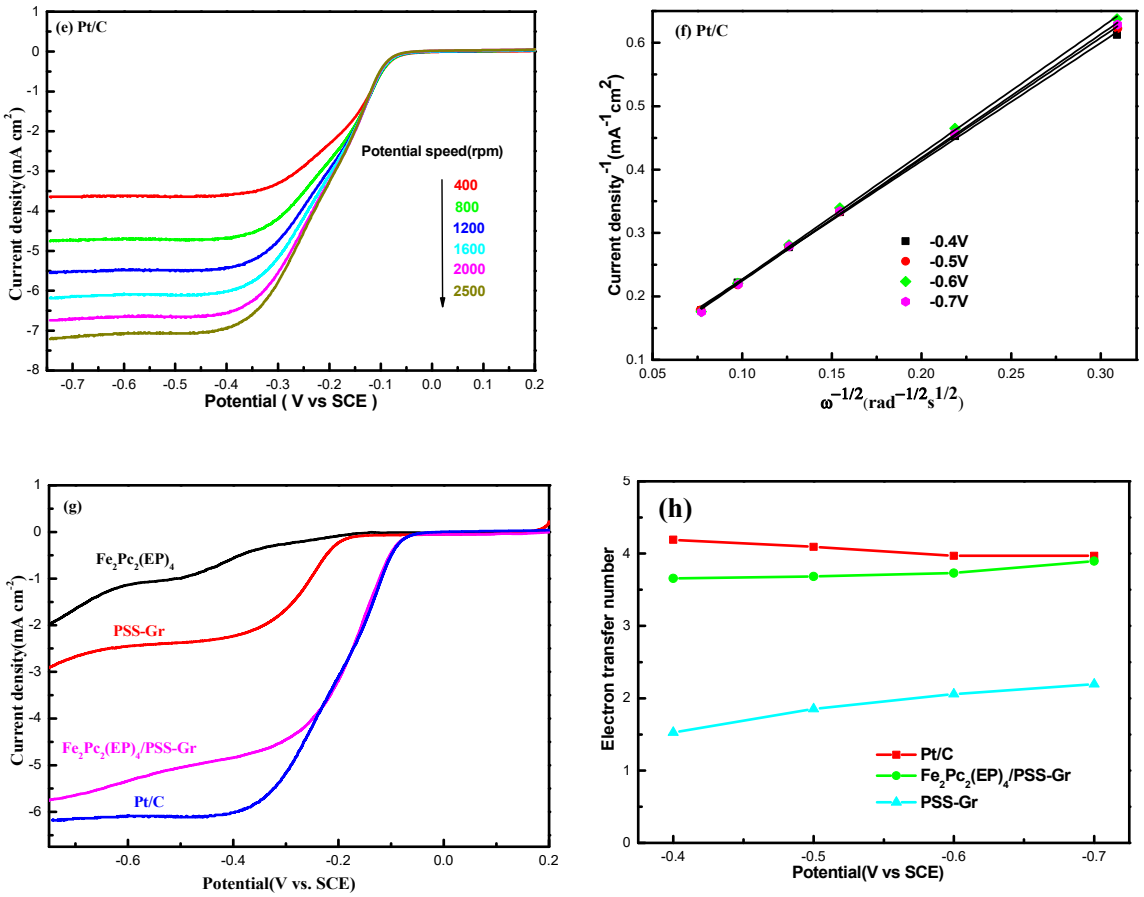

Figure 6. Electrocatalytic activities of Pt/C and $Fe_2Pc_2(EP)_4$/PSS-Gr at different rotation speed in O_2-saturated 0.1 M KOH; (**a**), (**c**), (**e**), (**g**) the linear sweep voltammetry (LSV) curve; (**b**), (**d**), (**f**) Koutecky-Levich (K-L) plots; (**h**) the number of electrons transferred.

The cyclic voltammetry curves of Pt/C and $Fe_2Pc_2(EP)_4$/PSS-Gr were further investigated, revealing reveal the cross-effect in an O_2 saturated 0.1 M NaOH solution containing 3 M CH_3OH. As shown in Figure 7, the oxygen reduction peak of Pt/C catalyst at −0.20 V decreased significantly for the oxygen reduction reaction after adding methanol into the system, and a methanol oxidation peak appeared at 0.0 V. However, the peak current density and peak potential had no significant difference for the $Fe_2Pc_2(EP)_4$/PSS-Gr catalyst under the same conditions. The results indicate that the $Fe_2Pc_2(EP)_4$/Gr catalyst had a good methanol-tolerant performance in an alkaline medium in the presence of methanol.

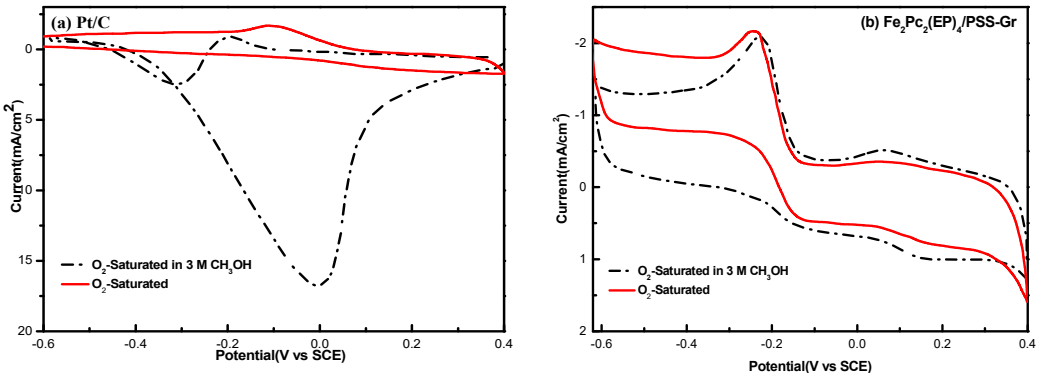

Figure 7. Cyclic voltammetry (CV) curves of $Fe_2Pc_2(EP)_4$/PSS-Gr in O_2-saturated in a 0.1 M KOH solution and O_2-saturated 0.1 M KOH solution with 3 M methanol. (**a**) Pt/C, and (**b**) $Fe_2Pc_2(EP)_4$/Gr.

A mechanism was proposed for ORR catalyzed by $Fe_2Pc_2(EP)_4$/PSS-Gr based on the experiment results and references (Figure 8). The electron transfer number n for $Fe(II)_2Pc_2(EP)_4$/PSS-Gr was 3.89 which was calculated by the Koutecky-Levich (K-L) equation. The results indicated that ORR mainly underwent a direct four electron pathway to result in OH^- production. First, the O_2 molecule was bonded to the central metal ion Fe(II) (d-filling of t_{2g}^6 e_g^0) of the MN_4-type $Fe(II)_2Pc_2(EP)_4$ macrocyclic system by bridge adsorption [16,17]. Bridge adsorption can coordinate one oxygen molecule with two central metal ions Fe(II), so it can form more stable peroxide intermediates, which are more conducive to oxygen-oxygen bond (O-O) breaking [25,46,47]. The electrons on the π electron conjugated structure $Pc_2(EP)_4$ migrate to the central metal ion Fe(II) and then to the O_2 molecule, to form an adduct $Fe(III)_2Pc_2(EP)_4{\cdot}O_2^-$, which showed the structure of Fe(III)-O-O-Fe(III) peroxo-species. The breaking of the O-O linkage for Fe(III)-O-O-Fe(III) peroxo species is expected to facilitate in the formation of OH^- ions. The electrons on PSS-Gr then migrated to $Fe(III)_2Pc_2(EP)_4$ and $Fe(III)_2Pc_2(EP)_4$ was reduced to $Fe(II)_2Pc_2(EP)_4$ [19,32,33]. Therefore, the π electron conjugated structure of the MN_4-type phthalocyanine macrocyclic system strongly influenced the one-step four-electron electrocatalytic process for ORR, and it effectively reduced the overpotential of the oxide reduction reaction [25]. Moreover, the performance of $M_2Pc_2(EP)_4$ catalysts was lower than that of the metallophthalocyanines with trifluoro methyl linkages [25]. The linkage of highly electrophilic groups, like trifluoro methyl groups, to the macrocycles dramatically enhanced the electrocatalytic performance. The comparison of the performances of $M_2Pc_2(EP)_4$ catalysts used in this work and in the reported article also points out the importance of the bridging units in the ball-type structure. More significantly, PSS-Gr dramatically enhanced the electrocatalytic activity of $M_2Pc_2(EP)_4$. PSS-Gr provide pathway for fast electron transferring and to prevent the aggregation of $M_2Pc_2(EP)_4$ catalysts. $M_2Pc_2(EP)_4$ were loaded on the surface of PSS-Gr to enhance the catalytic activity and stability for the ORR, based on the π-π supramolecular interaction between MPcs molecules and graphene. The results indicated that PSS-Gr enhanced the catalytic activity and stability of $M_2Pc_2(EP)_4$ for the ORR based on the π-π supramolecular interaction.

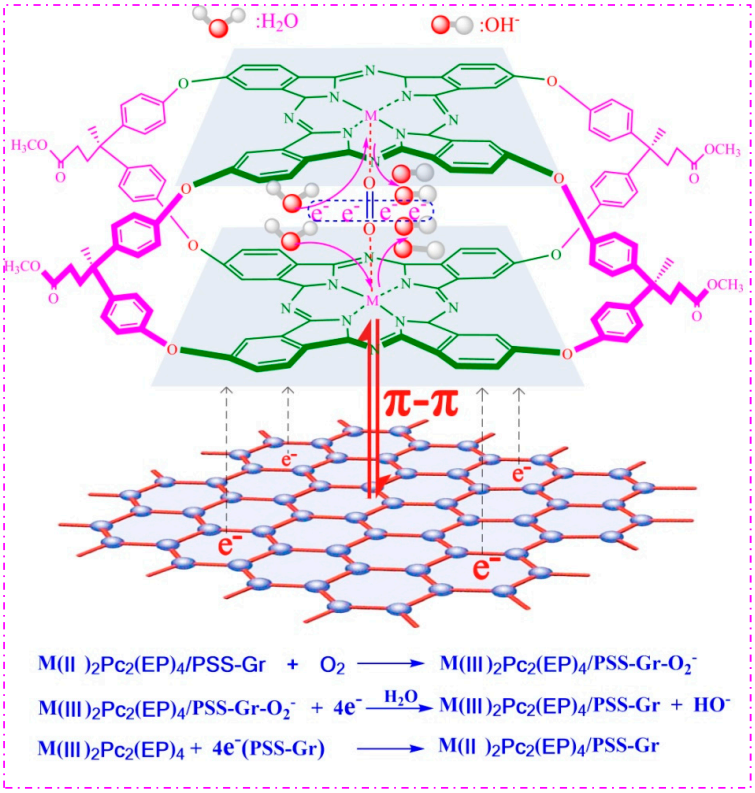

Figure 8. Mechanism for the oxygen reduction reaction (ORR) catalyzed by $Fe_2Pc_2(EP)_4$/PSS-Gr.

4. Conclusions

Composites of PSS-graphene-wrapped binuclear ball-type metallophthalocyanines with methoxy substituents ($M_2Pc_2(EP)_4$, M = Fe(II), Co(II) and Zn(II)) were synthesized to enhanced the electrocatalytic activity for the oxygen reduction reaction of $M_2Pc_2(EP)_4$. Compared to the commercial Pt/C catalysts, the $M_2Pc_2(EP)_4$/PSS-Gr composites had a high electrocatalytic activity. The π electron conjugated structure of the MN_4-type phthalocyanine macrocyclic system strongly influenced the four-electron electrocatalytic process. PSS-Gr enhance the catalytic activity and stability of the $M_2Pc_2(EP)_4$ composites, based on the π-π supramolecular interaction between MPcs molecules and graphene. PSS-Gr provide a pathway for fast electron transferring and prevent the aggregation of $M_2Pc_2(EP)_4$ catalysts. The results indicated that the catalytic performance of $M_2Pc_2R_n$ could be enhanced by the modification of the π electron conjugated structure of $M_2Pc_2(EP)_4$ and carbon materials.

Author Contributions: Conceptualization, G.Z., and L.B.; validation, G.Z., L.B.L., and Y.Z.; formal analysis, G.Z.; data curation, W.Z.; writing—original draft preparation, B.L.; writing—review and editing, G.Z., and W.Z.; visualization, T.L.; supervision, W.C.; project administration, G.Z.; funding acquisition, G.Z., W.Z. All authors have read and agreed to the published version of the manuscript.

Funding: This research received no external funding.

Acknowledgments: This research was supported by the Natural Science Foundation of Shaanxi Province (No. 2019JM-527), the National Natural Science Foundation of China (61604120, 21501139).

Conflicts of Interest: The authors declare no conflict of interest.

References

1. Guo, Y.; Jiang, Z.Q.; Wang, X.B.; Ying, W.; Chen, D.; Liu, S.H. Zwitterion threaded metal–organic framework membranes for direct methanol fuel cells. *J. Mater. Chem. A* **2018**, *6*, 19547–19554. [CrossRef]
2. Gago, A.S.; Acosta, D.M.; Arriaga, L.G.; Vante, N.A. Carbon supported ruthenium chalcogenide as cathode catalyst in a microfluidic formic acid fuel cell. *J. Power. Sources* **2011**, *196*, 1324–1328. [CrossRef]
3. Gong, L.Y.; Yang, Z.Y.; Li, K.; Xing, W.; Liu, C.P.; Ge, J.J. Recent development of methanol electrooxidation catalysts for direct methanol fuel cell. *J. Energy. Chem.* **2018**, *27*, 1618–1628. [CrossRef]
4. Ge, X.; Liu, Y.; Goh, F.T.; Hor, T.A.; Zong, Y.; Xiao, P. Dual-phase spinel $MnCo_2O_4$ and spinel $MnCo_2O_4$/nanocarbon hybrids for electrocatalytic oxygen reduction and evolution. *ACS. Appl. Mater. Interfaces* **2014**, *6*, 12684–12691. [CrossRef] [PubMed]
5. Xu, S.; Kim, Y.; Park, J.; Higgins, D.; Shen, S.J.; Schindler, P. Extending the limits of Pt/c catalysts with passivation-gas-incorporated atomic layer deposition. *Nat. Cat.* **2018**, *1*, 624–630. [CrossRef]
6. Rosli, N.F.; Carmen, C.; Martinez, M.; Latiff, N.M. Layered $PtTe_2$ Matches Electrocatalytic Performance of Pt/C for Oxygen Reduction Reaction with Significantly Lower Toxicity. *ACS. Sustain. Chem. Eng.* **2018**, *6*, 7432–7441. [CrossRef]
7. Whittingham, M.S. Lithium batteries and cathode materials. *Chem. Rev.* **2018**, *104*, 4271–4302. [CrossRef]
8. Morozan, A.; Campidelli, S.; Filoramo, A.; Jousselme, B.; Palacin, S. Catalytic activity of cobalt and iron phthalocyanines or porphyrins supported on different carbon nanotubes towards oxygen reduction reaction. *Carbon* **2011**, *49*, 4839–4847. [CrossRef]
9. Özer, L.M.; Altındal, A.; Özkaya, A.R.; Salih, B.; Bekaroglu, Ö. Synthesis, characterization, OFET and electrochemical properties of novel dimeric metallophthalocyanines. *Dalton. Trans.* **2013**, *42*, 6633–6644. [CrossRef]
10. Zhang, R.L.; Wang, J.; Xu, B.; Huang, X.Y.; Xu, Z.; Zhao, J.S. Investigation of binuclear metal phthalocyanines as electrocatalysts for Li/$SOCl_2$ battery. *J. Electrochem. Soc.* **2012**, *159*, H704–H710. [CrossRef]
11. Moraes, F.C.; Cabral, M.F.; Machado, S.A.; Mascaro, L.H. Electrocatalytic Behavior of Glassy Carbon Electrodes Modified with Multiwalled Carbon Nanotubes and Cobalt Phthalocyanine for Selective Analysis of Dopamine in Presence of Ascorbic Acid. *Electroanalysis* **2008**, *20*, 851–857. [CrossRef]

12. Odabaş, Z.; Altındal, A.; Özkaya, A.R.; Salih, B.; Bekaroglu, Ö. Novel ball-type homo-and hetero-binuclear phthalocyanines with four 1, 10- methylenedinaphthalen-2-ol bridges: Synthesis and characterization, electrical and gas sensing properties and electrocatalytic performance towards oxygen reduction. *Sens. Actuators B Chem.* **2010**, *145*, 355–366. [CrossRef]
13. Hyun, K.; Ueno, T.; Panomsuwan, G.; Li, O.L.; Saito, N. Heterocarbon nanosheets incorporating iron phthalocyanine for oxygen reduction reaction in both alkaline and acidic media. *Phys. Chem. Chem. Phys.* **2016**, *18*, 10856–10863. [CrossRef] [PubMed]
14. Xu, G.F.; Li, Z.F.; Wang, S. Planar polyphthalocyanine cobalt absorbed on carbon black as stable electrocatalysts for direct methanol fuel cell. *J. Power. Sources* **2010**, *195*, 4731–4735. [CrossRef]
15. Chen, J.M.; Zou, K.Y.; Ding, P.; Deng, J. Conjugated Cobalt Polyphthalocyanine as the Elastic and Reprocessable Catalyst for Flexible Li-CO_2 Batteries. *Adv. Mater.* **2018**, *31*, 1805484. [CrossRef] [PubMed]
16. Gu, J.Y.; Cai, Z.F.; Wang, D. Single molecular imaging of Iron-Phthalocyanine catalyzed oxygen reduction reaction by in situ scanning tunneling microscopy. *ACS Nano* **2016**, *10*, 8746–8750. [CrossRef] [PubMed]
17. Xu, Z.W.; Kang, L.; Wang, R.Y.; Duan, X.T.; Liu, Q.Q.; Zhang, R.L. Electrochemical Effects of Lithium-Thionyl Chloride Battery by Central Metal Ions of Phthalocyanines-Tetraacetamide Complexes. *J. Electrochem. Soc.* **2017**, *164*, A3628–A3632. [CrossRef]
18. Peng, Y.X.; Li, Z.P.; Xia, D.G.; Zheng, L.R.; Liao, Y.; Li, K. Probing the influence of the center atom coordination structure in iron phthalocyanine multi-walled carbon nanotube-based oxygen reduction reaction catalysts by X-ray absorption fine structure spectroscopy. *J. Power. Sources* **2015**, *291*, 20–28. [CrossRef]
19. Li, T.; Peng, Y.; Li, K.; Zhang, R.; Zheng, L.; Xia, D. Enhanced activity and stability of binuclear iron (III) phthalocyanine on graphene nanosheets for electrocatalytic oxygen reduction in acid. *J. Power. Sources* **2015**, *293*, 511–518. [CrossRef]
20. Yasemin, C.; Emel, E.; Fatih, D.; Ali, R.Ö.; Bekir, S.; Özer, B. Synthesis, characterization, electrochemistry and VOC sensingproperties of novel ball-type dinuclear metallophthalocyanines. *Sens. Actuators B* **2014**, *202*, 1137–1147.
21. Kakı, E.; Altındal, A.; Salih, B.; Bekaroğlu, Ö. Synthesis, characterization and gas sensing properties of novel homo and hetero binuclear ball-type phthalocyanines. *Dalton. Trans.* **2015**, *44*, 8293–8299.
22. Tolbin, A.Y.; Ivanov, A.V.; Tomilova, L.G.; Zefirov, N.S. Synthesis of 1,2-bis(3,4-dicyanophenoxymethyl)benzene and binuclear zinc phthalocyaninesof clamshell and ball types. *J. Porphyr. Phthalocyan* **2003**, *7*, 162–166. [CrossRef]
23. Tolbin, A.Y.; Ivanov, A.V.; Tomilova, L.G.; Zefirov, N.S. Preparation of 1,2-bis(3,4-dicyanophenoxymethyl)benzene and the binuclear zinc phthalocyaninederived from it. *Mendeleev. Commun.* **2002**, *12*, 96–97. [CrossRef]
24. Bekaroˇglu, Ö.; Jiang, J. *Functional Phthalocyanine Molecular Materials*; Springer: Berlin/Heidelberg, Germany, 2010; Volume 135, pp. 105–136.
25. Git, N.K.; Özen, Ü.E.; Özer, M.; Salih, B.; Özkaya, A.R.; Glu, Ö.B. Electrocatalytic Activity of Novel Ball-Type Metallophthalocyanines with Trifluoro Methyl Linkages in Oxygen Reduction Reaction and Application as Zn-Air Battery Cathode Catalyst. *Electrochim. Acta* **2017**, *233*, 237–248.
26. Beck, F.; Dammert, W.; Beiss, J.; Hiller, H.; Tolster, R. Electrocatalysis of oxygen cathode by metal-phthalocyanine and metal-dibenzotetraazaannulene. *Z. Naturforsch.* **1973**, *28*, 1009–1021.
27. Oliveira, M.A.C.; Mecheri, B.; D'Epifanio, A.; Placidi, E.; Arciprete, F.; Valentini, F. Graphene oxide nanoplatforms to enhance catalytic performance of iron phthalocyanine for oxygen reduction reaction in bioelectrochemical systems. *J. Power. Sources.* **2017**, *356*, 381–388. [CrossRef]
28. Liu, X.M.; Xu, T.; Li, Y.L.; Zang, Z.G.; Peng, X.S.; Wei, H.Y. Enhanced X-ray photon response in solution-synthesized $CsPbBr_3$ nanoparticles wrapped by reduced graphene oxide. *Sol. Energy Mater. Sol. Cells* **2018**, *187*, 249–254. [CrossRef]
29. Liu, L.; Zheng, K.; Yan, Y.; Cai, Z.H.; Lin, S.X.; Hu, X.B. Graphene Aerogels Enhanced Phase Change Materials prepared by one-pot method with high thermal conductivity and large latent energy storage. *Sol. Energy Mater. Sol. Cells* **2018**, *185*, 487–493. [CrossRef]
30. Kusuma, J.; Balakrishna, R.G.; Patil, S.; Jyothi, M.S.; Chandan, H.R.; Shwetharani, R. Exploration of Graphene oxide nanoribbons as excellent electron conducting network for third generation solar cells. *Sol. Energy Mater. Sol. Cells* **2018**, *183*, 211–219. [CrossRef]

31. Dai, L.M.; Chang, D.W.; Baek, J.B.; Lu, W. Carbon Nanomaterials for Advanced Energy Conversion and Storage. *Small* **2012**, *8*, 1130–1166. [CrossRef]
32. Cui, L.; Lv, G.; Dou, Z. Fabrication of iron phthalocyanine/Graphene micro/nanocomposite by solvothermally assisted π–π assembling method and its application for oxygen reduction reaction. *Electrochim. Acta* **2013**, *106*, 272–278. [CrossRef]
33. Zhang, X.; Feng, Y.; Tang, S.; Feng, W. Preparation of a Graphene oxide–phthalocyanine hybrid through strong π–π interactions. *Carbon* **2010**, *48*, 211–216. [CrossRef]
34. Zhang, G.; Liu, B.L.; Zhou, H.W.; Yang, Y.; Chen, W.X.; Zhao, J.S. Graphene Wrapped Phthalocyanine: Enhanced Oxidative Desulfurization for Dibenzothiophene in Fuel. *Appl. Organometallic. Chem.* **2018**, *32*, a4477. [CrossRef]
35. Liu, D.; Peng, J.H.; Li, Z.Y.; Liu, B.; Wang, L. Improvement in the mechanical properties, proton conductivity, and methanol resistance of highly branched sulfonated poly(arylene ether)/Graphene oxide Grafted with flexible alkylsulfonated side chains nanocomposite membranes. *J. Power. Sources* **2018**, *378*, 451–459. [CrossRef]
36. Zhang, Y.; Wu, H.K.; Zhao, W.; Li, X.M.; Yin, R.; Qian, L. Iron (II) phthalocyanine nanoclusters - Graphene sandwich composite for oxygen reduction reaction catalysts. *Mater. Des.* **2017**, *130*, 366–372. [CrossRef]
37. Cao, R.G.; Thapa, R.; Kim, H.; Xu, X.D.; Kim, M.G.; Li, Q. Promotion of oxygen reduction by a bio-inspired tethered iron phthalocyanine carbon nanotube-based catalyst. *Nat. Commun.* **2013**, *4*, 2076. [CrossRef]
38. Järvinen, P.; Sampsa, K.; Hämäläinen, M.; Harju, A. Self-Assembly and Orbital Imaging of Metal Phthalocyanines on a Graphene Model Surface. *J. Phys. Chem. C* **2014**, *118*, 13320–13325. [CrossRef]
39. Serov, A.; Artyushkova, K.; Andersen, N.I. Original Mechanochemical Synthesis of Non-Platinum Group Metals Oxygen Reduction Reaction Catalysts Assisted by Sacrificial Support Method. *Electrochim. Acta* **2015**, *179*, 154–160. [CrossRef]
40. Jaouen, F.; Herranz, J.; Lefèvre, M. Cross-Laboratory Experimental Study of Non-Noble-Metal Electrocatalysts for the Oxygen Reduction Reaction. *ACS. Appl. Mater. Interfaces* **2009**, *1*, 1623–1639. [CrossRef]
41. Jin, H.G.; Jiang, X.; Irina, A.; Clair, S.; Valérie, M.; Chendo, C. Microwave-mediated synthesis of bulky lanthanide porphyrin–phthalocyanine triple-deckers: Electrochemical and magnetic properties. *ACS Inorg. Chem.* **2017**, *6*, b03056. [CrossRef]
42. Tejerina, L.; Nazeeruddin, M.K.; GRätzel, M.; Torres, T. Role of the bulky aryloxy Group at the non-peripheral position of phthalocyanines for dye sensitized solar cells. *ChemPlusChem* **2017**, *82*, 132–135. [CrossRef] [PubMed]
43. Chen, R.; Li, H.; Chu, D. Unraveling Oxygen Reduction Reaction Mechanisms on Carbon-Supported Fe-Phthalocyanine and Co-Phthalocyanine Catalysts in Alkaline Solutions. *J. Phys. Chem. C* **2009**, *113*, 20689–20697. [CrossRef]
44. Guo, J.; He, H.; Chu, D. OH-Binding Effects on Metallophthalocyanine Catalysts for O_2, Reduction Reaction in Anion Exchange Membrane Fuel Cells. *Electrocatalysis* **2012**, *3*, 252–264. [CrossRef]
45. Oberst, J.L.; Thorum, M.S.; Gewirth, A.A. Effect of pH and Azide on the Oxygen Reduction Reaction with a Pyrolyzed Fe Phthalocyanine Catalyst. *J. Phys. Chem. C* **2018**, *116*, 25257–25261. [CrossRef]
46. Özen, Ü.E.; Elvan, D.; Özer, M.; Glu, Ö.B.; Özkaya, A.R. Communication—High-Performance and Non-Precious Bifunctional Oxygen Electrocatalysis with Binuclear Ball-Type Phthalocyanine Based Complexes for Zinc-Air Batteries. *J. Electrochem. Soc.* **2016**, *163*, A2001–A2003. [CrossRef]
47. Tanaka, A.; Fierro, C.; Scherson, D.; Yaeger, E. Electrocatalytic aspects of iron phthalocyanine and its. mu.-oxo derivatives dispersed on high surface area carbon. *J. Phys. Chem.* **1987**, *91*, 3799–3807. [CrossRef]